Received: 9 November 2023 | Revised: 25 January 2024 | Accepted: 5 February 2024

DOI: 10.1002/aoc.7412

FULL PAPER

Applied Organometallic Chemistry WILEY

Inclusion complexes of cucurbit[*n*]urils ($n = 7, 8$) with η^5-cyclopentadienyl methyl tricarbonyl molybdenum(II) and their use in epoxidation catalysis

Patrícia Neves[1] | **Ana C. Gomes**[1] | **Rodrigo P. Monteiro**[1] | **Mirela J. Santos**[1] | **Anabela A. Valente**[1] | **André D. Lopes**[2] | **Isabel S. Gonçalves**[1] | **Martyn Pillinger**[1]

[1]CICECO - Aveiro Institute of Materials, Department of Chemistry, University of Aveiro, Campus Universitário de Santiago, Aveiro, Portugal

[2]CCMar and Department of Chemistry and Pharmacy, FCT, University of the Algarve, Faro, Portugal

Correspondence
Anabela A. Valente and Martyn Pillinger, CICECO - Aveiro Institute of Materials, Department of Chemistry, University of Aveiro, Campus Universitário de Santiago, Aveiro 3810-193, Portugal.
Email: atav@ua.pt and mpillinger@ua.pt

Funding information
CICECO - Aveiro Institute of Materials, Grant/Award Numbers: UIDB/50011/2020, UIDP/50011/2020, LA/P/0006/2020; FCT/MCTES, Grant/Award Number: CEECIND/02128/2017; European Social Fund, Grant/Award Number: 2020.04758.BD

There are very few known examples of supramolecular compounds comprising molybdenum species hosted inside the portals/cavities of cucurbit[*n*]urils (CB*n*). In this work, CB7 and CB8 macrocycles have been studied as hosts for the carbonyl complex $[CpMo(CO)_3Me]$ (**1**) ($Cp = \eta^5$-C_5H_5). Compounds were isolated in the solid state and characterized as genuine 1:1 inclusion complexes (**1**@CB*n*) by elemental and thermogravimetric analyses, powder X-ray diffraction, scanning electron microscopy, $^{13}C\{^1H\}$ cross-polarization magic-angle spinning NMR, FT-IR, Raman, and diffuse reflectance UV–Vis spectroscopies. The host–guest structures can act as supramolecular precatalysts for olefin epoxidation. Based on the model reaction of *cis*-cyclooctene with hydroperoxide oxidants (*tert*-butylhydroperoxide or hydrogen peroxide), the structural features of **1**@CB*n* as well as the operating conditions influence the catalytic process. The metal species in **1**@CB*n* undergo oxidative decarbonylation in situ, giving oxidized metal species that are catalytically active for olefin epoxidation. The type of oxidant and solvent influences the catalytic activity and stability. **1**@CB8 was more stable than **1**@CB7 with regard to catalyst recycling and reuse. Based on the substrate scope investigation, for relatively large olefins, such as the fatty acid methyl ester methyl oleate, the size of the macrocyclic host may be a determining factor for catalytic activity.

KEYWORDS
carbonyl complexes, cucurbiturils, inclusion compounds, molybdenum, olefin epoxidation

1 | INTRODUCTION

The development of industrially viable transition metal catalysts is largely dependent on the optimization of catalyst activity, selectivity, and stability.[1,2] Traditionally, this has been achieved through ligand design strategies that aim to modify the structure of ligands in the first coordination sphere to fine-tune steric, electronic, and geometric factors.[3–5] Further tweaks in catalyst performance can be achieved by introduction of a second coordination sphere,[5] with one popular tactic being the encapsulation of a metal catalyst (the guest) in a molecular container (the host).[6,7] A key attraction of the host–guest approach is that catalytic properties can be altered

without modification of the first-sphere ligands because inclusion complex formation is founded on noncovalent interactions such as van der Waals forces, the "hydrophobic effect," hydrogen bonding, release of conformational strain, and entropic gains from extrusion of water from the host cavity.

Cavitands, defined as synthetic organic compounds that contain enforced cavities large enough to accommodate simple molecules or ions,[8] are particularly versatile containers for molecular transition metal catalysts. The five main classes of organic cavitands and cavitand scaffolds are calixarenes, resorcinarenes, cyclotriveratrylenes, cyclodextrins (CDs), and cucurbiturils (CBs).[9] The following examples serve to highlight some of the possibilities of host–guest catalysis with these organic containers: (i) β-CD enhanced the stability of methyltrioxorhenium (VII) used as a catalyst for the oxidation of indigo blue dye with H_2O_2[10]; (ii) a copper(I)-carbene azide-alkyne cycloaddition catalyst was inhibited through encapsulation by CB7 and activated by its release by chemical signals[11]; (iii) by forming a ternary complex with $[Ru(bpy)_3]^{2+}$ and methyl viologen, CB10 accelerated electron transfer between the ruthenium (II) photocatalyst and the organic substrate[12]; and (iv) an inclusion complex between $[Rh(nbd)_2]BF_4$ (nbd = norbornadiene) and an amide-functionalized resorcin[4]arene catalyzed the hydrogenation of nbd into norbornene as the main product, while the nonincluded metal complex converted nbd to a partially reduced dimer.[13]

In previous work, we encapsulated the cyclopentadienyl molybdenum tricarbonyl complexes $[CpMo(CO)_3X]$ ($Cp = \eta^5$-C_5H_5; X = Cl, CH_2CONH_2, CH_2-pC_6H_4-CO_2CH_3) in native β-CD and methylated derivatives to prepare host–guest catalysts for the epoxidation of *cis*-cyclooctene (Cy8), used as a model olefin.[14–16] Under the reaction conditions employed, the tricarbonyl catalyst precursor reacts with the oxidant, either *tert*-butylhydroperoxide (TBHP) or H_2O_2, to give the active Mo^{VI} catalyst, which is typically an oxo complex such as $[CpMoO_2Cl]$ or a peroxo complex such as $[CpMoO(O_2)Cl]$.[17,18] Depending on the type of host and cosolvent (if used), the catalyst systems were either homogeneous, biphasic liquid–liquid, or heterogeneous. The 1:1 adduct of β-CD with $[CpMo(CO)_3(CH_2CONH_2)]$ was insoluble and could be recycled without loss of catalytic activity.[14] In contrast, for the biphasic system $[CpMo(CO)_3(CH_2$-pC_6H_4-$CO_2CH_3)]$@TRIMEB/TBHP/TFT/H_2O (TRIMEB = permethylated β-CD, TFT = α,α,α-trifluorotoluene), the catalyst-containing aqueous phase could be reused directly after decantation of the organic phase containing the reaction products.[16] Finally, although the free complex $[CpMo(CO)_3Cl]$ is mainly inactive as a catalyst precursor with aqueous H_2O_2 as oxidant, the introduction of β-CD to the system instilled significant activity.[15]

The examples given above show that the formation of host–guest complexes is a viable strategy to introduce a second coordination sphere around molybdenum carbonyl complexes and thereby modify their catalytic behavior. To the best of our knowledge, only CDs have so far been examined as organic cavitands for these types of catalyst precursors. In the present work, inclusion complexes between $[CpMo(CO)_3Me]$ and CBs (CB7 and CB8) have been prepared and studied as host–guest catalysts for the epoxidation of the olefins Cy8, cyclododecene (Cy12), and methyl oleate (MeOle) (Scheme 1). The main finding from this study is that catalytic performance (activity, selectivity, and recycling) changes with the nature of the host.

2 | EXPERIMENTAL SECTION

2.1 | Starting materials, reagents, and substrates

For synthesis, the following materials were purchased from Sigma-Aldrich (unless indicated otherwise) and used as received: molybdenum hexacarbonyl (Sigma-Aldrich), 2.4 M sodium cyclopentadienylide in tetrahydrofuran (THF), iodomethane (99%), glycoluril, paraformaldehyde, hydrochloric acid, acetone (p.a., Scharlau), and anhydrous ethanol (Carlo Erba). THF, hexane, and diethyl ether were dried by standard procedures, distilled under nitrogen, and kept over 4 Å molecular sieves. For catalysis, the following materials were purchased from Merck products-

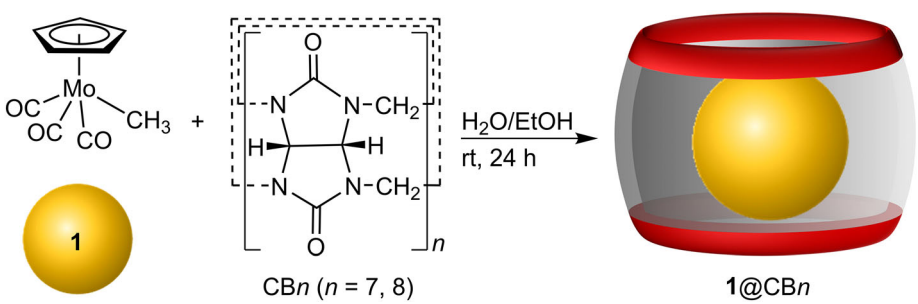

SCHEME 1 Preparation of inclusion compounds **1**@CB7 and **1**@CB8.

Life Technologies (unless indicated otherwise) and used as received: *cis*-cyclooctene (95%, Alfa Aesar), MeOle (99%), cyclododecene (mixture of cis/trans isomers, 96%), anhydrous TFT (≥99%), 5.5 M TBHP in decane (containing <4 wt.% water), 70 wt.% aqueous TBHP ($TBHP_{aq}$), 30 wt.% H_2O_2, acetonitrile (99.9%, Panreac), ethanol (99.9%, Carlo Erba), hexane (99%, Carlo Erba), undecane (≥99%), and methyl decanoate (99%). The synthesis and characterization of CB7 (approximate composition $C_{42}H_{42}N_{28}O_{14}{\cdot}11H_2O{\cdot}0.1HCl{\cdot}0.5(CH_3COCH_3)$) and CB8 (approximate composition $C_{48}H_{48}N_{32}O_{16}{\cdot}7H_2O{\cdot}3HCl{\cdot}1.5(CH_3COCH_3)$) were described previously.[19,20]

2.2 | Instrumentation

Microanalyses (CHNS) were performed with a Truspec Micro CHNS 630-200-200 instrument. ICP-OES analyses for Mo were performed at the Central Analysis Laboratory, University of Aveiro, using a Horiba JobinYvon Activa M spectrometer (detection limit of ~20 μg dm^{-3}). Prior to analysis, solid samples (10 mg) were digested using 1 mL HF and 1 mL HNO_3 with microwave-assisted heating at 180°C. Powder X-ray diffraction (PXRD) data were collected at room temperature (rt) on a Malvern Panalytical Empyrean diffractometer (Malvern Panalytical, Malvern, UK) equipped with a spinning flat plate sample holder and a PIXcel 1D detector set at 240 nm from the sample, in a Bragg–Brentano para-focusing optics configuration. Cu-K$\alpha_{1,2}$ X-radiation ($\lambda_1 = 1.5406$ Å) was used, with the X-ray tube operated at the voltage of 45 kV and the current of 40 mA. Samples were step-scanned in continuous mode from 5° to 70° (2θ) with step sizes of 0.02°, a counting time of 50 s per step, and automatic data acquisition (X'Pert Data Collector v4.2 software). Thermogravimetric analyses (TGA) were carried out using a HITACHI STA300 system from rt to 800°C at a heating rate of 5°C min^{-1} under a continuous flow of nitrogen. Scanning electron microscopy (SEM) images were obtained on a Hitachi SU-70 microscope equipped with a Bruker Quantax 400 detector operating at 15 kV. Samples were prepared by deposition on aluminum sample holders followed by carbon coating using an Emitech K 950 carbon evaporator.

Attenuated total reflectance (ATR) FT-IR spectra were obtained in the spectral range of 350 to 4000 cm^{-1} using Mattson-7000 or Bruker Tensor 27 spectrometers equipped with a Specac Golden Gate Mk II ATR accessory having a diamond top plate and KRS-5 focusing lenses (resolution 4 cm^{-1}, 256 scans). Raman spectra were recorded on a Bruker MULTIRAM instrument equipped with a Nd:YAG laser, with an excitation wavelength of 1064 nm (1000 scans, 4 cm^{-1} resolution). Solid-state $^{13}C\{^1H\}$ cross-polarization (CP) magic-angle spinning (MAS) NMR spectra were recorded at 100.62 MHz on a Bruker Avance 400 spectrometer, using 3.5 μs ^1H 90° pulses, a 2 ms contact time, a spinning rate of 10 kHz, and 5 s recycle delays. Chemicals shifts are quoted in ppm relative to TMS. Diffuse reflectance UV–Vis spectra were recorded at rt in the range 190–900 nm with a scan speed of 200 nm min^{-1} using a JASCO V-780 spectrophotometer equipped with a JASCO ISV-469 integrating sphere, with Spectralon as reference material.

2.3 | Synthesis

2.3.1 | Methyltricarbonyl(η^5-cyclopentadienyl)molybdenum(II) (**1**)

The complex $[CpMo(CO)_3Me]$ (**1**) was prepared as previously described by reaction of NaCp (5.52 mmol; 2.3 mL of a 2.4 M solution in THF) with $Mo(CO)_6$ (1.00 g, 3.79 mmol) in dry THF (20 mL) under an atmosphere of nitrogen, which gave $Na[CpMo(CO)_3]$, followed by addition of MeI (0.70 mL, 11.3 mmol).[21] FT-IR and ^1H NMR spectral data for **1** agreed with literature results.[21,22] ATR FT-IR (cm^{-1}): ν = 3115 (w), 2981 (w), 2903 (w), 2816 (w), 2003 (vs, ν(C≡O)), 1889 (vs, ν(C≡O)), 1460 (w), 1421 (m), 1354 (w), 1262 (w), 1159 (m), 1109 (w), 1083 (w), 1061 (w), 1009 (m), 924 (w), 914 (w), 821 (vs), 580 (m), 558 (vs), 481 (vs), 449 (vs), 403 (m), 354 (m). Raman (cm^{-1}): ν = 3125 (m), 3103 (m), 2986 (m), 2907 (m), 2817 (w), 2021 (m), 2007 (m), 1904 (s), 1425 (m), 1356 (w), 1230 (w), 1164 (m), 1110 (s), 1063 (m), 1011 (w), 915 (w), 825 (w), 769 (w), 612 (w), 581 (w), 485 (w), 455 (m), 440 (s), 407 (m), 357 (m), 337 (m), 176 (m), 106 (vs). $^{13}C\{^1H\}$ CP MAS NMR: δ = 241.6 (Mo-CO), 229.8 (Mo-CO), 93.9 (Cp), −23.4 (Mo-CH_3).

2.3.2 | **1**@CB7

A solution of **1** (0.04 g, 0.14 mmol) in ethanol (0.5 mL) was added to an aqueous suspension (20 mL) of CB7 (0.20 g, 0.14 mmol). After stirring the mixture for 24 h at rt, a pale cream precipitate was obtained, which was isolated by centrifugation (6000 rpm) and vacuum-dried. Anal. Calcd for $C_{42}H_{42}N_{28}O_{14}{\cdot}C_9H_8MoO_3{\cdot}14H_2O$: C, 36.56; H, 4.69; N, 23.41; Mo, 5.7%. Found: C, 36.27; H, 5.00; N, 23.52; Mo, 5.2%. TGA of **1**@CB7 revealed a mass loss of 14.2% from rt up to 250°C (calcd for **1**·CB7·$14H_2O$: 15.0% H_2O). ATR FT-IR (cm^{-1}): ν = 3454 (s, br), 3005 (w), 2920 (w), 2016 (m, ν(C≡O)), 1921 (s, ν(C≡O)), 1716 (vs, ν(C=O)), 1639 (sh), 1462 (vs), 1417 (s), 1373 (s), 1316 (s), 1296 (m), 1253 (m), 1226 (vs), 1183 (s), 1152 (m),

1028 (w), 990 (sh), 964 (s), 901 (w), 860 (w), 823 (m), 796 (vs), 754 (m), 666 (m), 626 (w), 584 (w), 566 (w), 500 (m), 440 (w), 358 (s). Raman (cm^{-1}): $\nu = 3129$ (w), 3104 (w), 2993 (m), 2933 (s), 2830 (w), 2018 (m), 1927 (s), 1743 (m), 1495 (w), 1422 (s), 1382 (m), 1324 (m), 1283 (w), 1230 (w), 1202 (w), 1189 (w), 1137 (w), 1112 (m), 1059 (w), 1044 (w), 1011 (w), 972 (w), 900 (w), 829 (s), 753 (m), 711 (m), 684 (w), 656 (m), 471 (m), 458 (m), 438 (s), 366 (m), 336 (m), 289 (m), 275 (w), 185 (m), 94 (vs), 62 (vs). $^{13}C\{^1H\}$ CP MAS NMR: $\delta = 224.0$ (Mo-CO), 156.0 (N(CO)N), 96.5 (Cp), 71.3 (CH), 52.8 (CH_2), −18.9 (Mo-CH_3).

2.3.3 | 1@CB8

A solution of **1** (15.6 mg, 0.06 mmol) in ethanol (0.5 mL) was added to an aqueous suspension (20 mL) of CB8 (0.10 g, 0.06 mmol). After stirring the mixture for 24 h at rt, a pale cream precipitate was obtained, which was isolated by centrifugation (6000 rpm) and vacuum-dried. Anal. Calcd for $C_{48}H_{48}N_{32}O_{16}{\cdot}C_9H_8MoO_3{\cdot}13.5H_2O{\cdot}2.5HCl$: C, 35.59; H, 4.48; N, 23.30; Mo, 5.0%. Found: C, 35.01; H, 4.48; N, 23.74; Mo, 4.45%. TGA of **1**@CB8 revealed a mass loss of 12.8% from rt up to 250°C (calcd for **1**·CB8·13.5H_2O·2.5HCl: 12.6% H_2O). ATR FT-IR (cm^{-1}): $\nu = 3462$ (s, br), 2998 (w), 2912 (w), 2016 (m, ν(C≡O)), 1918 (s, ν(C≡O)), 1715 (vs, ν(C=O)), 1639 (sh), 1458 (vs), 1418 (s), 1374 (s), 1314 (s), 1286 (m), 1222 (vs), 1183 (vs), 1152 (m), 1028 (w), 990 (sh), 966 (s), 830 (m), 799 (vs), 751 (m), 664 (m), 627 (w), 587 (w), 560 (w), 488 (m), 439 (w). Raman (cm^{-1}): $\nu = 3107$ (w), 2987 (w), 2942 (s) 2911 (m), 2021 (m), 1930 (m), 1766 (m), 1735 (m), 1427 (m), 1382 (m), 1329 (w), 1288 (w), 1228 (w), 1202 (w), 1110 (m), 1044 (w), 974 (w), 918 (w), 904 (w), 833 (s), 753 (m), 658 (m), 439 (s), 366 (m), 335 (m), 278 (w), 174 (s). $^{13}C\{^1H\}$ CP MAS NMR: $\delta = 239.2$ (Mo-CO), 225.2 (Mo-CO), 155.9 (N(CO)N), 91.9 (Cp), 71.4 (CH), 53.4 (CH_2), −21.9 (Mo-CH_3).

2.4 | Catalytic olefin epoxidation

The catalytic reactions were carried out in tubular borosilicate batch reactors possessing a valve for sampling and pear-shaped bottoms (~12 mL capacity), loaded with an adequate magnetic bar for stirring at 1000 rpm. Typically, an initial Mo:olefin:oxidant molar ratio of 1:100:152 was used (0.7 M olefin). The timing of the catalytic reactions was started from the moment that the loaded reactors were immersed in a stirred oil bath heated to 70°C or 90°C. A separate reactor was prepared for each reaction time point. After the desired reaction time, the reactors were cooled to rt, and the reaction mixtures were analyzed using an Agilent 7820 A gas chromatograph equipped with a DB-5 capillary column (30 m × 0.25 mm × 0.25 μm; H_2 as the carrier gas) and an FID detector. The product quantifications were based on calibrations using undecane (for Cy8 and Cy12) or methyl decanoate (for MeOle) as internal standards. The reaction products were identified by GC–MS (GC-2010 Pluz/GCMS-QP2010 Ultra [Shimadzu]) with a ZB-5m column (He as the carrier gas).

Control tests were carried out using CB7 or CB8 (without Mo) in a mass quantity equivalent to that of **1**@CB7 and **1**@CB8, respectively, under typical conditions. The oxidant efficiency for the systems **1**@cucurbit [*n*]urils (CB*n*)/Cy8/TBHP ($n = 7$, 8) was checked by iodometric titration after reaction at 6 h/90°C.

The reaction mixtures were solid–liquid; the solid was separated by centrifugation (5000 rpm), thoroughly washed four times with hexane or ethanol, dried overnight under atmospheric conditions, and finally vacuum-dried (~0.1 bar) for 1 h at 60°C. The used solids were characterized by ATR FT-IR spectroscopy and SEM with Mo mapping. The stability of the catalysts was further studied by reusing the solids in consecutive batch runs (recovering the solids after each run as described above), keeping the initial catalyst:olefin:oxidant mass ratio constant.

To quantify the contribution of soluble metal species to olefin conversion, contact tests were carried out as follows: The mixture **1**@CB*n*/TFT/TBHP was heated at 90°C for 6 h, with stirring at 1000 rpm; afterward, the reaction mixture was passed through a 0.2 μm PTFE membrane filter to separate the solid catalyst from the liquid phase (LP); the olefin (Cy8) was then added to this LP in an initial amount equivalent to 0.7 M (as performed under the standard conditions); and the mixture was left to react for 6 h at 90°C with stirring at 1000 rpm. The evolution of the homogeneous phase reaction was monitored by GC as described above.

3 | RESULTS AND DISCUSSION

3.1 | Synthesis and characterization of the inclusion compounds

To isolate CB7 and CB8 adducts containing encapsulated **1**, solutions of **1** in ethanol were mixed with the respective CB partially dissolved/suspended in water, with an initial **1**:CB molar ratio of 1:1 (Scheme 1). The resultant cream-colored solids (designated as **1**@CB7 and **1**@CB8) were isolated by centrifugation of the mixtures, followed

by vacuum-drying at rt. CHN microanalyses and Mo determination by ICP-OES indicated that the initial **1**: CB*n* molar ratio was retained in the isolated products. To the best of our knowledge, only one other publication has described the encapsulation of an organomolybdenum compound in CBs, namely, Cp_2MoCl_2 in CB7 and CB8.[23] Harding and coworkers ascertained through ^1H NMR titration experiments that the metallocene formed 1:1 host–guest complexes with both hosts.

Figure 1 shows the TGA curves of **1**, the native hosts CB7 and CB8, and the compounds **1**@CB*n*. Complex **1** shows two main weight loss steps from rt up to 530°C: a mass loss of 48.6% between 80°C and 180°C (DTG [derivative] peak maximum at 157°C) and a loss of 8.0% between 470°C and 525°C (DTG_{max} = 500°C). The low final residual mass of 33.1% indicates that a combination of decomposition and sublimation took place during the experiment, probably during the first weight loss step, that is, decarbonylation of **1** may occur simultaneously with sublimation of the complex. As-prepared CB7 and CB8 display almost identical TGA curves, with a 17.9–20.1% mass loss between rt and 170°C due to removal of water (DTG_{max} = 65°C) and, in the case of CB8, acetone, an abrupt macrocycle decomposition around 420°C, and finally a protracted mass loss of 6–7% between 500°C and 700°C. The TGA curves of **1**@CB7 and **1**@CB8 are similar to each other, but differ from those of the pure hosts. First, both compounds have reduced water/acetone contents that culminate in mass losses of 14.2% and 12.8%, respectively, at 250°C. Second, the main decomposition step is identified by DTG_{max} values of 335°C for **1**@CB7 and 375°C for **2**@CB8, that is, 45–85°C lower than the corresponding values for the as-prepared hosts. We attribute this decrease in CB thermal stability to the promoting effect of guest decomposition. Indeed, the TGA curves of **1**@CB7 and **1**@CB8 do not exhibit any weight loss steps in the range 100–250°C resulting from sublimation/decarbonylation of **1** (either "free" or encapsulated). Hence, sublimation/decarbonylation of **1** is inhibited by encapsulation in the CB hosts, with the decomposition of the organometallic guest taking place concurrently with CB decomposition above 250°C. Another consequence of the simultaneous decomposition of CB hosts and organometallic guest is the larger relative mass loss observed, that is, 78.1–81.2% in the range 250–500°C for **1**@CB*n* versus 49.0–50.1% in the range 300–500°C for CB*n*. Overall, the TGA results for **1**@CB*n* provide good support for the presence of inclusion compounds in which the $[CpMo(CO)_3Me]$ molecules are confined within the CB cavities.

PXRD confirmed the poorly crystalline nature of the as-synthesized CB7 sample (Figure 2b). It is noteworthy, however, that the trace matches with the intensity envelope observed in the PXRD pattern of a more crystalline CB7 sample reported previously,[20] indicating that the two samples have the same basic structure (CB packing arrangement), albeit with different degrees of long-range

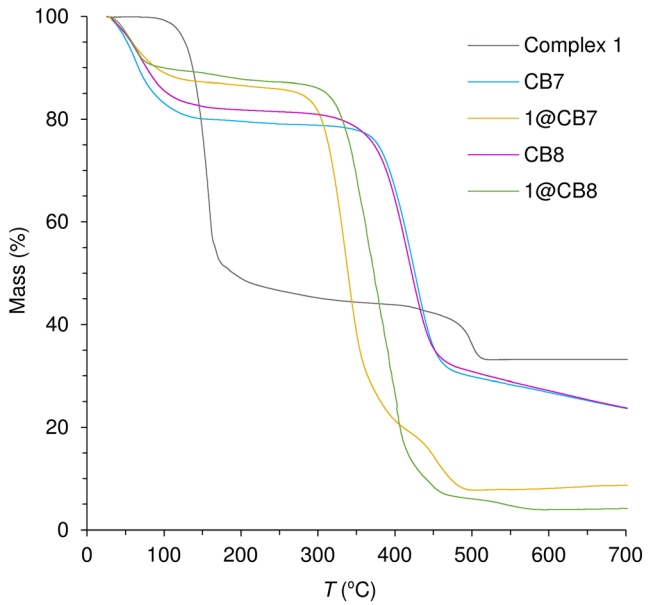

FIGURE 1 Thermogravimetric analysis curves, obtained under N_2, of **1**, CB*n*, and **1**@CB*n*.

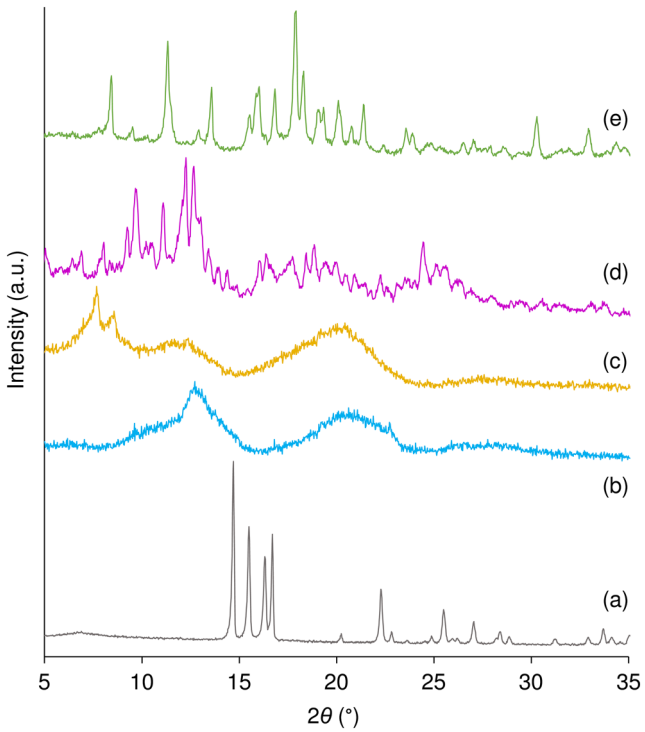

FIGURE 2 Powder X-ray diffraction patterns in the range 5–35° 2θ of (a) **1**, (b) CB7, (c) **1**@CB7, (d) CB8, and (e) **1**@CB8.

order. The compound **1**@CB7 also produced a halo pattern characteristic of an amorphous solid (Figure 2c). This pattern is, nevertheless, different from that for CB7 in that two narrower peaks are observed at 7.7° and 8.5° 2θ, possibly indicating a different packing arrangement for the host molecules and hence the presence of a genuine inclusion complex with **1**. For **1**@CB8, PXRD provides stronger support for the formation of an inclusion complex in the solid state because the sample is microcrystalline, with several quite sharp reflections in the range of 5–35° 2θ (Figure 2e), and the pattern is distinct from that for microcrystalline CB8 (Figure 2d). The PXRD patterns of **1**@CB7 and **1**@CB8 do not contain reflections that match with those for pure **1** (Figure 2a), suggesting the absence of nonincluded complex.

The ATR FT-IR and FT-Raman spectra of **1**@CB7 and **1**@CB8 contain the characteristic bands of the host macrocycle, with no significant shifts being registered (Figure 3). The ATR FT-IR spectra show two bands in the carbonyl (C≡O) stretching region at 1918–1921 and 2016 cm^{-1}. The bands are shifted to higher frequency by 32–39 and 13 cm^{-1}, respectively, relative to those for nonincluded complex **1** in the solid state. The shape of the lower frequency ν(C≡O) band changes from being very broad and asymmetric for **1** (with an extended shoulder on the low-frequency side) to relatively sharp and symmetric for **1**@CB7 and **1**@CB8. These spectral changes are consistent with inclusion complexation. Thus, the asymmetric broadening of the ν(C≡O) band for **1** may be due to solid-state intermolecular interactions (CH···O and CH···π, which are known to be present in carbonyl/Cp-containing organometallics[24]), which would not be present for the inclusion compounds. Second, the blueshifts observed for the ν(C≡O) bands of **1**@CB*n* mirror those typically observed when comparing solution and solid–state FT-IR spectra of organomolybdenum carbonyl complexes, thereby indicating that the organometallic guest complexes are in a "solution-like" isolated environment by encapsulation in the host cavities.[25,26] Similar blueshifts are observed for the Raman ν(C≡O) bands from 1904 and 2006 cm^{-1} for **1** to 1927–1930 and 2018–2021 cm^{-1} for the inclusion compounds. The vibrational spectra of the inclusion compounds contain some additional bands with weak-to-medium intensity attributable to the organometallic guest. In the ATR FT-IR spectra, bands at 500 and 566 cm^{-1} for **1**@CB7 and 488 and 560 cm^{-1} for **1**@CB8 are assigned as antisymmetric out-of-plane and in-plane MoCO deformation vibrations (cf. bands at 481 and 558 cm^{-1} for the free complex **1**).[27] Raman bands at 335–336 cm^{-1} (ν_s(MoCp)) and 1110–1112 cm^{-1} (ν_s(CC), Cp) for the inclusion compounds are essentially unshifted with respect to the corresponding bands for **1**.

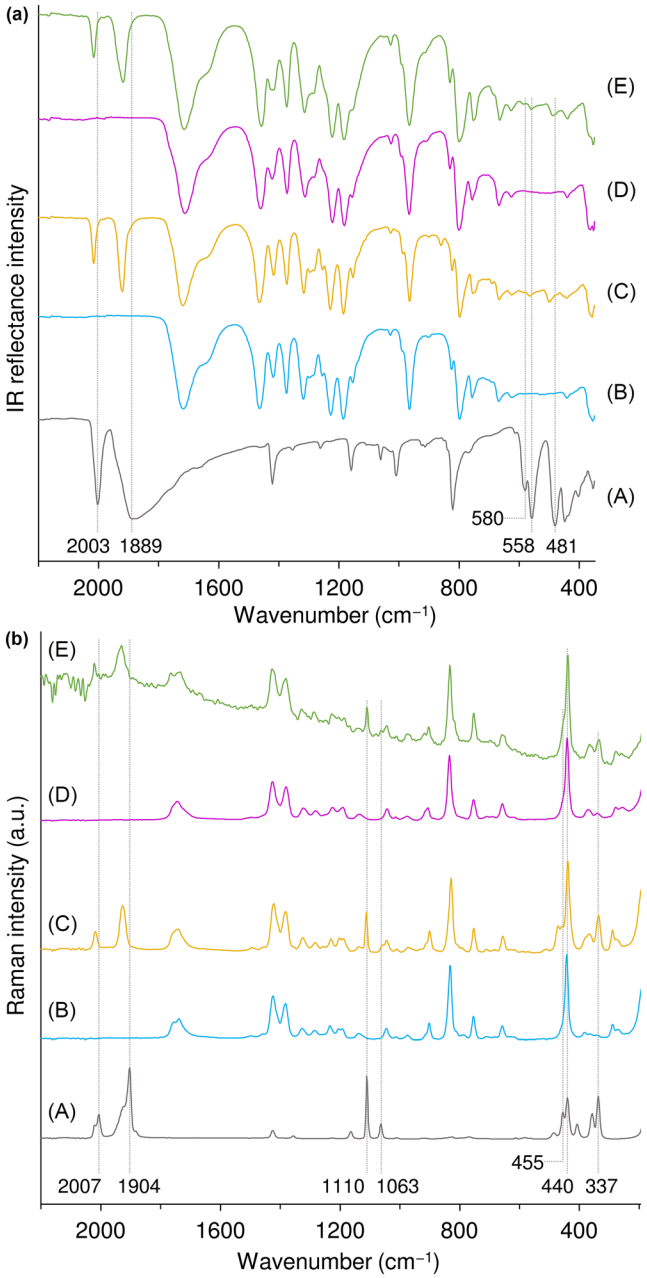

FIGURE 3 Attenuated total reflectance FT-IR (a) and Raman (b) spectra of (A) **1**, (B) CB7, (C) **1**@CB7, (D) CB8, and (E) **1**@CB8. The frequencies of selected bands for **1** are highlighted with dotted lines.

The $^{13}C\{^1H\}$ CP MAS NMR spectra of **1**@CB*n* show single, relatively sharp, peaks for the guest molecule, indicating that the inclusion compounds contain only one type of crystallographically distinct organometallic complex (Figure 4c,e). In the solid-state structure of **1**, the complex adopts the four-legged piano-stool geometry that is common for $CpML_4$ complexes.[21] Accordingly, the solid-state NMR spectrum of **1** shows one resonance at 229.8 ppm for the two equivalent CO ligands *cis* to the methyl group, one weaker peak at 241.6 ppm for the CO

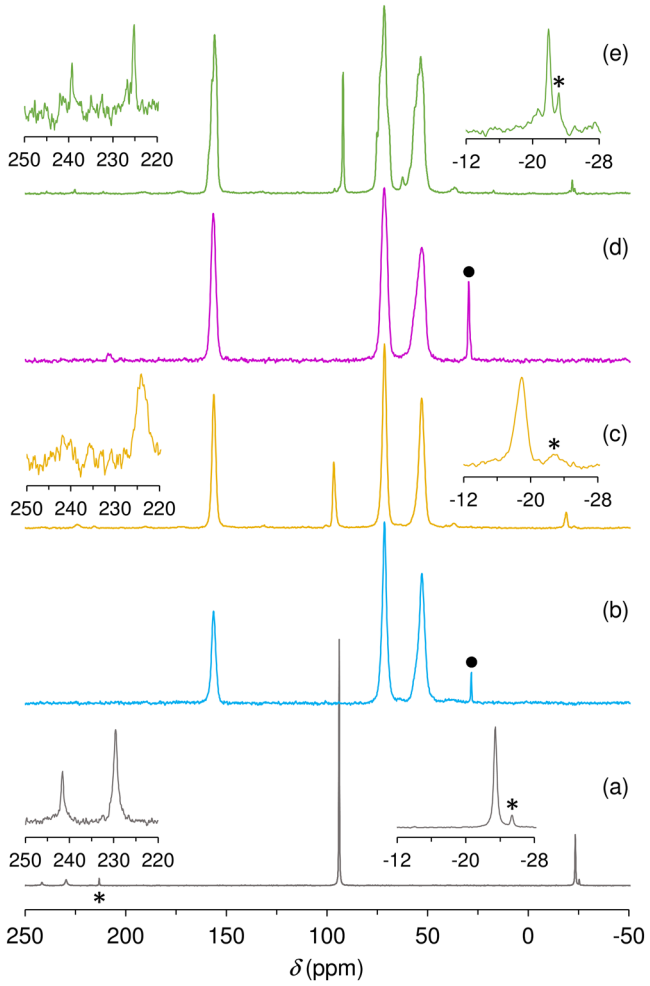

FIGURE 4 $^{13}C\{^1H\}$ cross-polarization magic-angle spinning NMR spectra of (a) [CpMo(CO)$_3$Me] (**1**), (b) CB7, (c) **1**@CB7, (d) CB8, and (e) **1**@CB8. The insets for **1** and **1**@CB*n* show expansions of the −28 to −12 ppm and 220 to 250 ppm regions. The signal identified with a filled circle is due to acetone present in the as-prepared CB*n*. Spinning sidebands are labelled with an asterisk.

ligand *trans* to the methyl group, and sharp signals at −23.4 and 93.9 ppm for the methyl and Cp groups, respectively (Figure 4a). Compared with the signals for **1**, the signals for **1**@CB*n* display mild shifts, both downfield ($\delta_{Me} = -18.9$ ppm for **1**@CB7 and −21.9 ppm for **1**@CB8; $\delta_{Cp} = 96.5$ ppm for **1**@CB7) and upfield ($\delta_{C\equiv O}$ [*cis* to Me] = 224.0 ppm for **1**@CB7 and 225.2 ppm for **1**@CB8; $\delta_{Cp} = 91.9$ ppm for **1**@CB8). Regarding the signals for the CB7 and CB8 carbons, the spectra of CB*n* (Figure 4b,d) and **1**@CB*n* are practically identical, showing single peaks centered at about 156.0 ppm for the C=O groups, 71.4 ppm for the CH groups, and 53.1 ppm for the bridging CH_2 groups.

The diffuse reflectance UV–Vis (250–850 nm) spectra of **1**, **1**@CB7, and **1**@CB8 are shown in Figure 5.

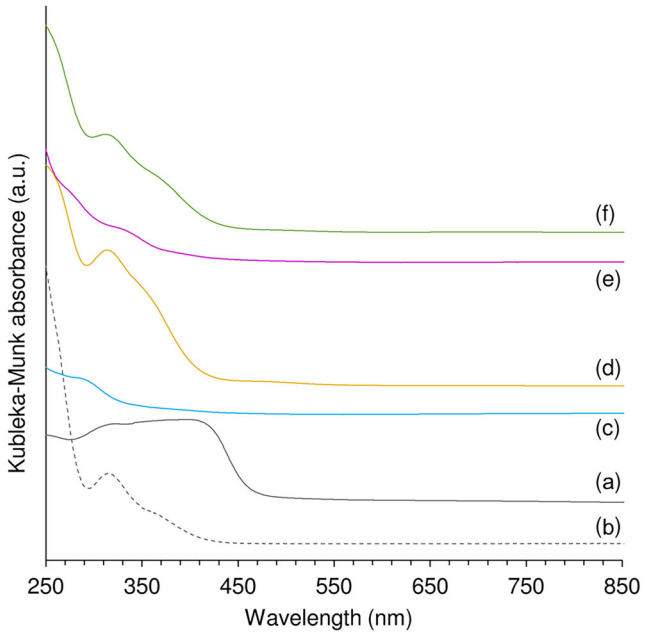

FIGURE 5 Solution UV–Vis spectra of **1** in ethanol (b) and solid-state diffuse reflectance UV–Vis spectra of [CpMo(CO)$_3$Me] (**1**) (a), CB7 (c), **1**@CB7 (d), CB8 (e), and **1**@CB8 (f).

Complex **1** exhibits a broad absorption feature that arises from the overlap of bands with maxima in the UV and visible regions (Figure 5a). A high energy component with λ_{max} ~323 nm is assigned to a metal-to-ligand charge transfer (MLCT) transition, while the very broad low energy absorption with λ_{max} ~400 nm (which gives rise to the lemon-yellow color of the complex) likely involves overlapping MLCT and ligand field bands. In the solution spectrum of **1** in ethanol, the former band is relatively more intense with $\lambda_{max} = 315$ nm, while the latter band appears as an unresolved shoulder (Figure 5b). In the UV–Vis range (250–850 nm), where electronic transitions for the two free CBs are absent (apart from weak shoulders at ~280 nm for CB7 and ~270/320 nm for CB8; Figure 5c,e), the spectra of the inclusion compounds (Figure 5d,f) resemble more closely the spectrum of **1** in ethanol than **1** in the solid state, with only a minor hypsochromic shift of 2–3 nm being observed for the main MLCT band. This is another pointer to the organometallic molecules being separated from each other by encapsulation within the isolated environment of the host cavities.

3.2 | Catalysis studies

The inclusion compounds **1**@CB7 and **1**@CB8 were first studied in the model epoxidation reaction of *cis*-cyclooctene (Cy8) at 70°C, using TBHP (decane solution)

as oxidant. Olefin epoxidation was highly favored in the presence of the **1**@CB*n* compounds (e.g., 85% Cy8 conversion at 24 h for **1**@CB7), with cyclooctene epoxide (Cy8O) being the sole product. Increasing the reaction temperature from 70°C to 90°C enhanced the reaction kinetics, which was faster for **1**@CB7 than for **1**@CB8 (Figure 6). Specifically, Cy8 conversion at 6 h was 67%/90% at 70°C/90°C for **1**@CB7 and 38%/46% at 70°C/90°C for **1**@CB8. At the higher temperature, complete conversion was reached within 24 h for **1**@CB7. The faster reaction kinetics for **1**@CB7 than **1**@CB8 does not seem to correlate with the CB*n* portal sizes. The kinetic diameter of Cy8 molecules is ~5.5 Å,[28] which is comparable with the portal diameter of CB7 (5.4 Å) and smaller than the diameter of CB8 (6.9 Å).[29] Faster reaction kinetics might therefore be expected for the CB8 inclusion compound, but this was not observed. Whereas the epoxide selectivity was always 100% at 70°C, differences in selectivity were found for the two catalysts used at 90°C. At the higher temperature and at 85–90% conversion, the epoxide selectivity was higher for **1**@CB7 (100% at 90% conversion, 6 h) than for **1**@CB8 (83% at 85% conversion, 24 h). A hydroxy-cyclooctene-type byproduct seems to be formed, which may occur via interaction of the olefin with organometal complexes possessing oxo ligands (M=O).[30]

Reactions were sluggish without molybdenum (blank test using Cy8/TBHP/CB*n*) or without oxidant (blank test using Cy8/**1**@CB*n*) (<8% conversion at 24 h/90°C). These results suggest that molybdenum and oxidant are required for the formation of the active oxidizing species, which agrees with mechanistic studies reported in the literature for Mo-catalyzed epoxidation systems.[18,31,32] It is generally accepted that TBHP coordinates to the metal center, which acts as a Lewis acid, with concomitant protonation of an oxo ligand (Mo=O), resulting in an active oxidizing species containing a moiety of the type {Mo(OH)(OOR)} (R = *tert*-butyl) which is involved in the oxygen atom transfer to the olefin to give the epoxide product (and *tert*-butanol as the coproduct of TBHP consumption). Scheme 2 shows a simplified representation of a general mechanism (based on literature studies) for the oxidation of [CpMo(CO)$_3$Me] (free or encapsulated) and catalytic activity of the resulting complexes in olefin epoxidation.[18,31,32] Accordingly, the reaction process is governed by a heterolytic mechanism involving the coordination of the reactant molecules to Mo-containing active species.

Apart from the reaction temperature, oxidant efficiency is another factor that influences the epoxidation process. Iodometric titration indicated that **1**@CB8 led to a greater unproductive decomposition of TBHP (i.e., not consumed for producing epoxide) than **1**@CB7 (~65% and 12% decomposition, respectively, at 6 h/90°C). The faster unproductive decomposition of the oxidant in the presence of **1**@CB8 correlates with the slower

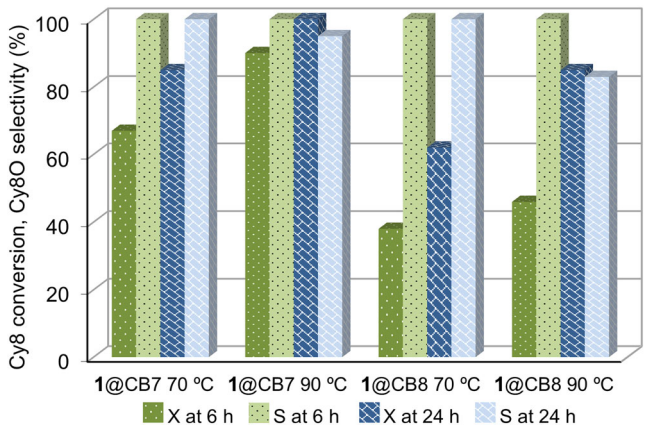

FIGURE 6 *cis*-Cyclooctene epoxidation in the presence of **1**@CB7 or **1**@CB8, at 6 h (dotted green bars) and 24 h (blue bars with bricks), using *tert*-butylhydroperoxide/α,α,α-trifluorotoluene at 70°C or 90°C (dark-colored bars = Cy8 conversion; light-colored bars = Cy8O selectivity).

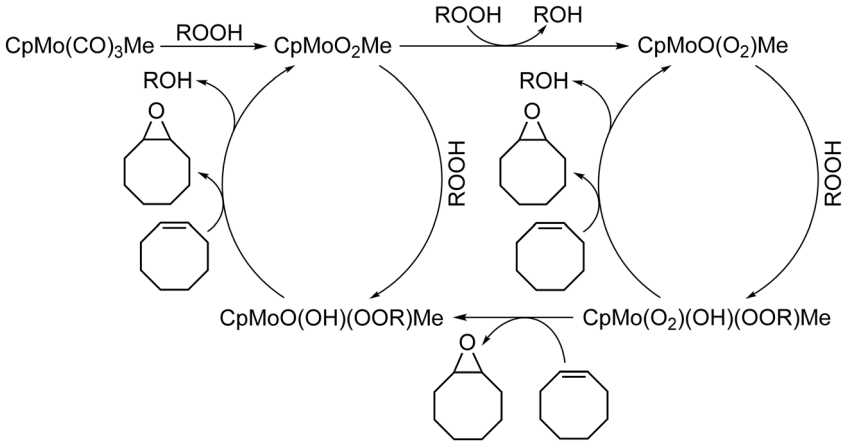

SCHEME 2 Simplified representation of a general mechanism (based on experimental and theoretical studies reported in the literature) for the oxidation of [CpMo(CO)$_3$Me] (free or encapsulated) and catalytic activity of the resulting complexes in olefin epoxidation with an alkyl hydroperoxide as oxidant (e.g., R = *tert*-butyl).

epoxidation reaction, likely because the unproductive decomposition of TBHP may reduce the instantaneous molar ratio of TBHP:Cy8, affecting the epoxidation reaction kinetics. The differences in TBHP efficiency and epoxide selectivity (discussed above) for the two **1**@CB*n* compounds may be partly due to differences in the structures of the active sites.

Several literature reports describe the application of complexes of the type $[CpMo(CO)_3X]$ (X = halide, alkyl) as catalyst precursors for olefin epoxidation.[18,21,27,31,33–35] These complexes may be oxidized to different types of metal species such as the mononuclear compounds $[CpMoO_2X]$, $[CpMoO(O_2)X]$, and $[CpMoO_2(OOtBu)]$, or dinuclear compounds like $[(CpMoOX)_2(\mu\text{-}O)]$, which may possess different intrinsic activities.[18,27,31,33–36] Some studies report the formation of unidentified, blue-colored compounds from complex **1**, which were either inactive[18] or active[36] for Cy8/TBHP conversion. In the present work, to gain insight into the types of metal species formed, complex **1** was used as a catalyst precursor, and the product(s) of its in situ oxidation was (were) characterized.

When tested under identical conditions to those used for **1**@CB*n* (initial Mo:Cy8:TBHP molar ratio = 1:100:152), the free complex **1** was more active, leading to 100% conversion within 30 min at 70°C or 10 min at 90°C. However, the reaction mixture for **1** consisted of a solid and a yellow LP (not observed for **1**@CB*n*, as discussed below), suggesting that the catalytic process was homogeneous in nature. One of the main drawbacks of using homogeneous catalysts is the need for separation and recovery steps downstream of the reactor, such as solvent extraction of the reaction products from an ionic liquid solution containing the Mo-based catalyst.[21] The ATR FT-IR spectra of the solids recovered after a 2 h batch run at 70°C or 90°C with **1** were similar and roughly comparable with that described previously for a solid recovered from the reaction system **1**/Cy8/TBHP at 55°C.[36] A comparison of the spectra of the tricarbonyl precursor **1** and the recovered solids confirms that the former undergoes chemical transformation under the catalytic reaction conditions, with oxidative decarbonylation (ODC) leading to the disappearance of the ν(C≡O) bands (at 1889 and 2003 cm^{-1}) and Cp-centered absorptions (e.g., in-plane and out-of-plane CH deformation modes at 1009 and 821 cm^{-1}, and ν(CH) at 3115 cm^{-1})[27] and the appearance of several new bands that are attributed to vibrational modes of Mo=O (956 cm^{-1}), peroxo (~860 and 530 cm^{-1}), and Mo-O-Mo groups (617 and 664 cm^{-1}) (Figure 7). Hence, the data suggest that the oxidation of **1** with TBHP involves the loss of CO and Cp groups and the formation of oxo(peroxo)molybdenum species.

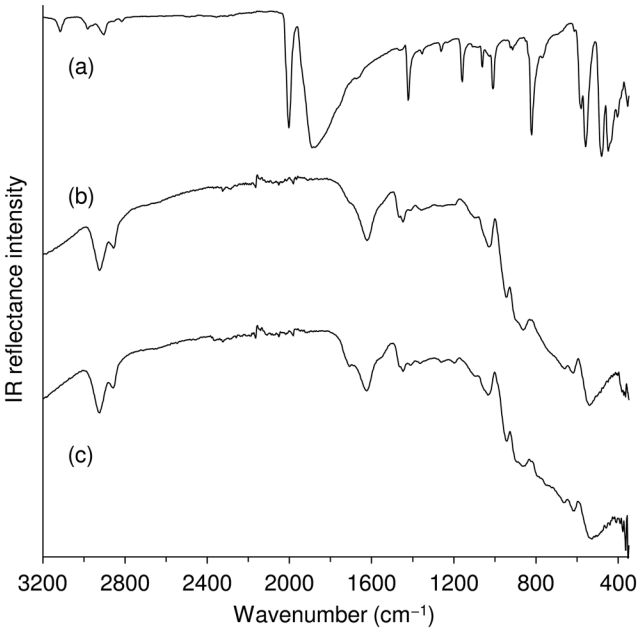

FIGURE 7 Attenuated total reflectance FT-IR spectra in the range of 350–3200 cm^{-1} of (a) **1** and the solids recovered after a 2 h batch run of the **1**/Cy8/*tert*-butylhydroperoxide/α,α,α-trifluorotoluene system at (b) 70°C and (c) 90°C.

The stability of the supramolecular compounds **1**@CB*n* was investigated by characterizing and reusing the solids recovered after catalytic runs. Comparison of the ATR FT-IR spectra of **1**@CB*n* with those for the recovered solids shows that ODC of the guest tricarbonyl complex took place in situ during the first catalytic run because there is a drastic reduction in the relative intensity of the ν(C≡O) bands, coupled with the appearance of a weak band at about 910 cm^{-1}, which is assigned to ν(Mo=O) (Figure 8). The latter assignment is supported by the observation that no similar band appears after using the pristine CBs (instead of **1**@CB*n*) in a catalytic run performed at 90°C (spectra labelled as CB*n*/90-r1 in Figure 8). The spectra for CB*n*/90-r1 confirm that the CB macrocycles are stable under the catalytic conditions. For **1**@CB*n*, the predominance of IR bands from the CB*n* hosts makes it difficult to draw further conclusions about the structures of the oxidized metal species. Nevertheless, based on the literature studies discussed above for **1**, one cannot rule out the possible formation of different types and amounts of metal species in **1**@CB7 versus **1**@CB8, which may possess different intrinsic activities and, consequently, catalytic performances (activity, selectivity, and oxidant efficiency).

For the precursor **1**@CB7, the spectra of the solids recovered after 6 h reaction at either 70°C or 90°C (labelled as *T*-r1 (6 h) in Figure 8) are similar, showing very weak ν(C≡O) bands at 1921 and 2015 cm^{-1}. These

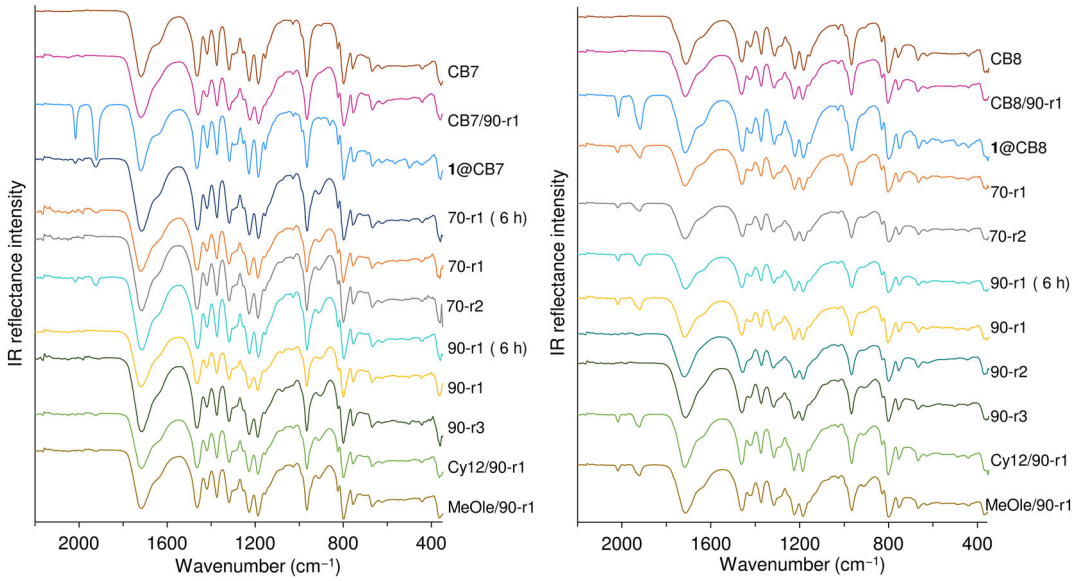

FIGURE 8 Attenuated total reflectance FT-IR spectra in the range of 350–2200 cm^{-1} of CB*n* and the corresponding recovered solids CB*n*/90-r1 ($n = 7$ [left panel] and 8 [right panel]), the inclusion compounds **1**@CB*n*, and the corresponding recovered solids *T*-r*i* (where *T* is the reaction temperature and *i* is the run number). In all cases, the oxidant was *tert*-butylhydroperoxide and the cosolvent was α,α,α-trifluorotoluene. Unless otherwise indicated, the substrate was Cy8 and the reaction time was 24 h.

bands completely disappear for solids recovered after 24 h reaction. A slightly different outcome was observed for **1**@CB8, where weak ν(C≡O) bands persist even for reaction times of 24 h and temperatures of 70°C or 90°C. After reusing these solids in a second catalytic run, weak ν(C≡O) bands were still present for the lower reaction temperature, while none were observed for the higher temperature (spectra labelled as *T*-r2 in Figure 8). The apparently faster ODC for **1**@CB7 versus **1**@CB8 correlates with the higher oxidant efficiency (productive TBHP consumption) of the former. Figure 8 shows that once complete ODC had occurred for **1**@CB7 or **1**@CB8 (i.e., after one run at 70°C or 90°C for **1**@CB7 and after two runs at 90°C for **1**@CB8), no further spectral changes were observed upon reuse of the solids (see the spectra labelled as 70-r2 and 90-r3 for **1**@CB7 and 90-r3 for **1**@CB8).

SEM and elemental (Mo) mapping by EDS were performed for the as-prepared and recovered inclusion compound catalysts (Figure 9). No drastic changes in morphology were observed, and the molybdenum distribution remained uniform.

To assess whether the catalytic processes with **1**@CB*n* were homogeneous and/or heterogeneous in nature, contact tests were carried out, which comprised treating **1**@CB*n* with TBHP/TFT for 6 h at 90°C, followed by filtration to remove the solid material, addition of Cy8 to the filtrate, and monitoring of any Cy8 conversion for a further 6 h. The LPs were colorless and led to sluggish results for **1**@CB7 (13% conversion for LP vs. 90% with no filtration) and **1**@CB8 (19% conversion for LP vs. 46% with no filtration), suggesting that the catalytic processes with **1**@CB*n* were essentially heterogeneous, that is, Mo active species were retained inside the host cavities rather than being leached into solution. The used catalysts could be recycled after separation from the reaction mixture via filtration or centrifugation. Each catalyst led to similar results for three consecutive 24 h batch runs at 90°C (100% conversion for **1**@CB7 and 85–87% conversion for **1**@CB8; Figure 10). As the reaction was very fast at the higher temperature of 90°C (which could lead to erroneous conclusions about the catalytic stability), catalyst recycling was also performed for the reaction temperature of 70°C (Figure 10). The results at 70°C suggest that **1**@CB8 was more stable (58–65% conversion for three consecutive 24 h batch runs) than **1**@CB7 (conversion dropped from 85% in run 1 to 66% in run 3). In parallel to that verified for **1**@CB8 in run 1 at 90°C, epoxide selectivity was less than 100% in subsequent runs at this temperature (Cy8O selectivity was in the range of 78–84%, at 24 h). For **1**@CB7, Cy8O selectivity was always >95% in consecutive batch runs.

The influences of the oxidant solution and solvent were studied for the more stable **1**@CB8 (Figure 11 and Table 1). The tested oxidant solutions were TBHP (TFT or MeCN as solvent), $TBHP_{aq}$ (TFT, MeCN, or H_2O as solvent), and H_2O_2 (MeCN or H_2O as solvent).

The TBHP/TFT system led to somewhat faster reaction kinetics than the $TBHP_{aq}$/TFT one, for example, 85% and 71% conversion at 24 h/90°C (Table 1). However,

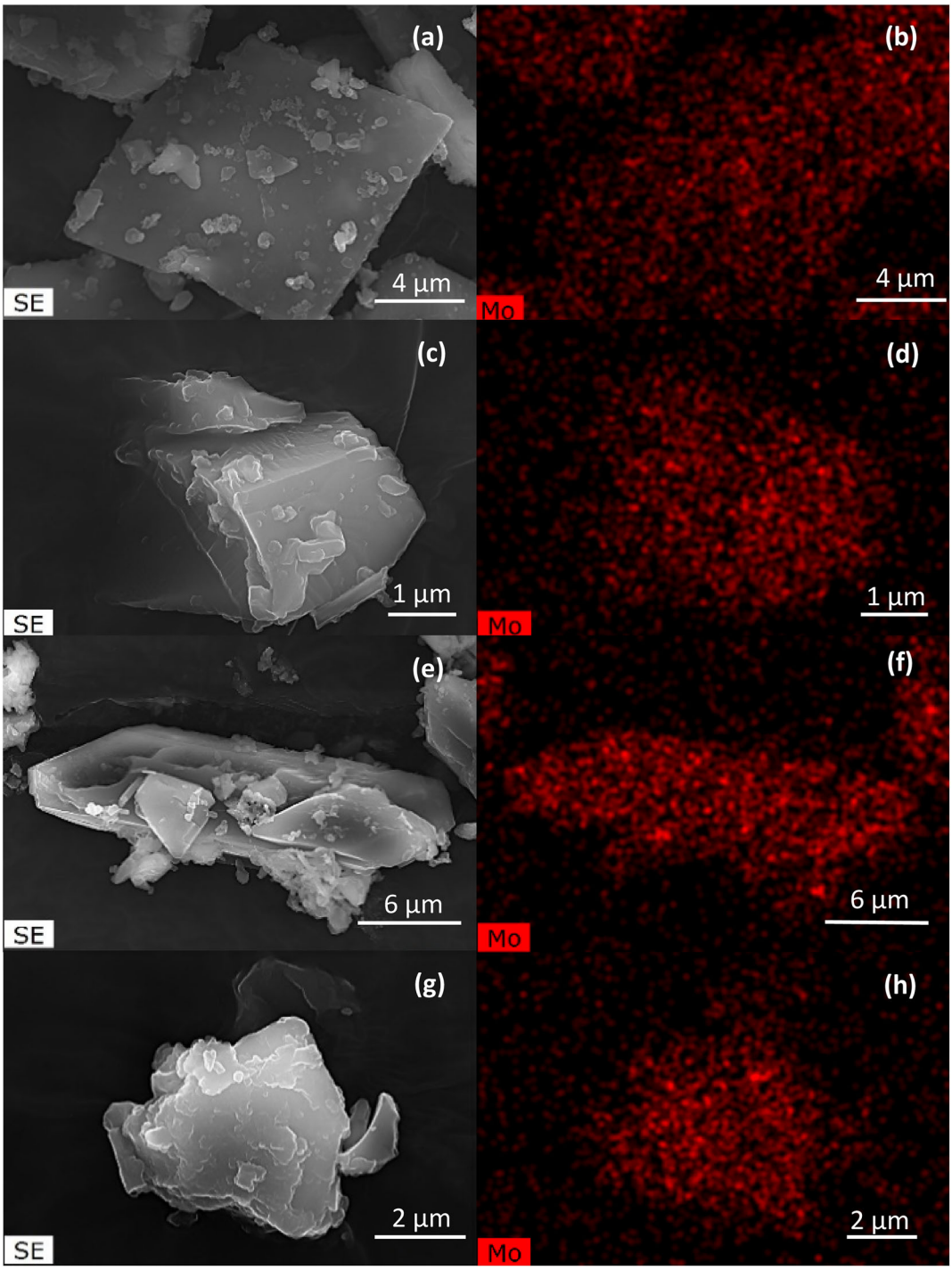

FIGURE 9 Scanning electron microscopy and Mo mapping images of fresh (a, b) and used (in catalysis; c, d) **1**@CB7 and of fresh (e, f) and used (in catalysis; g, h) **1**@CB8. Reaction conditions: oxidant = *tert*-butylhydroperoxide, cosolvent = α,α,α-trifluorotoluene, $T = 70°C$, $t = 24$ h.

while the catalytic activity was steady with TBHP/TFT (as discussed above), the $TBHP_{aq}$/TFT system led to loss of catalytic activity (and selectivity, at 90°C) over consecutive batch runs (conversion at 24 h in run 1/run 2/run 3 was 57%/40%/35% at 70°C and 71%/59%/53% at 90°C) (Figure 11 and Table 1). Hence, excess water seems to negatively affect the catalytic performance. The ATR FT-IR spectra of the solids recovered from the TBHP/TFT and $TBHP_{aq}$/TFT systems suggest that ODC was faster for the latter, because the ν(C≡O) bands disappeared within 24 h at 70°C or 90°C (and the ν(Mo=O) band appeared), whereas they remained present for TBHP/

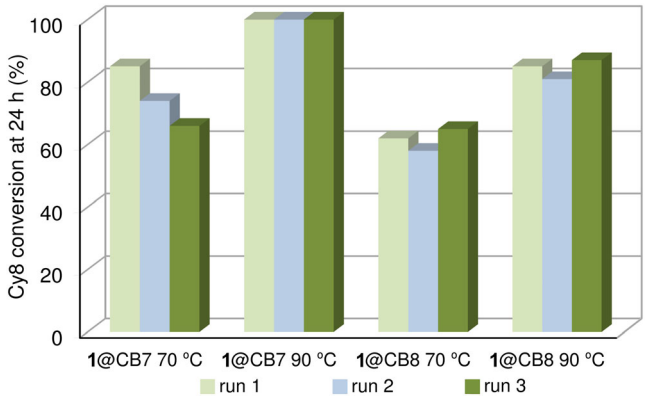

FIGURE 10 Consecutive catalytic runs of Cy8 epoxidation with *tert*-butylhydroperoxide as oxidant and α,α,α-trifluorotoluene as cosolvent, at 70°C or 90°C, in the presence of **1**@CB7 and **1**@CB8.

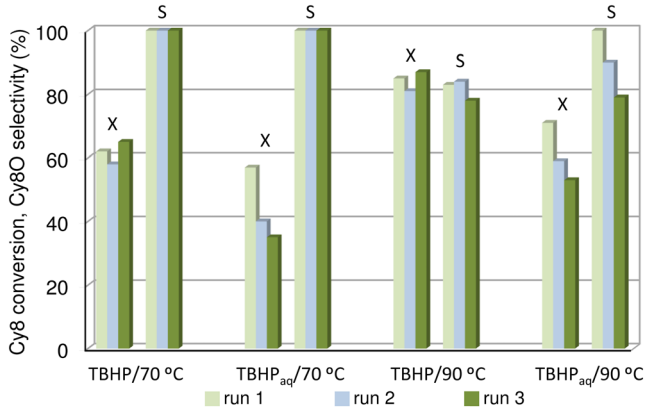

FIGURE 11 Epoxidation of Cy8 at 70°C and 90°C in the presence of **1**@CB8 using either *tert*-butylhydroperoxide (TBHP) (decane solution) or TBHP$_{aq}$ (aqueous solution) as the oxidant source and α,α,α-trifluorotoluene as cosolvent (X = conversion at 24 h, S = Cy8O selectivity).

TFT under similar conditions (Figure 12). Faster ODC may lead to faster formation of active oxidizing species, which may enhance the epoxidation reaction kinetics, but this was not verified for the (TBHP$_{aq}$ vs. TBHP)/TFT systems. Water is a protic coordinating solvent, and based on the above mechanistic considerations, it may compete with the reactants (olefin and oxidant) for coordination to the metal center, retarding the epoxidation reaction. However, this may be levelled off by the apparent faster ODC in the presence of water. On the other hand, the poorer catalytic stability using TBHP$_{aq}$/TFT may be partly due to the formation of different types of metal species for TBHP versus TBHP$_{aq}$.[37]

The above hypotheses are somewhat supported by the fact that the reaction of Cy8 using water as solvent, that is, TBHP$_{aq}$/H_2O, led to similar conversion at 24 h (61%) to that reached for (approximately anhydrous) TBHP/TFT (62%) at 70°C (Table 1), that is, the coordinating ability of water cannot solely explain the differences in catalytic performances. The ATR FT-IR spectrum of the solid recovered from the TBHP$_{aq}$/H_2O system confirmed that ODC was complete within 24 h (Figure 12), which may contribute positively to the epoxidation reaction kinetics at least in the first catalytic batch run. However, the catalytic stability was poor for the TBHP$_{aq}$/H_2O system (Cy8 conversion at 24 h/70°C for run 1/run 2/run 3 was 61%/39%/32%, and Cy8O selectivity was 100%/100%/88%), which (as suggested above) may be partly due to the formation of different types of (less stable/inactive) metal species in aqueous systems.

With TBHP or TBHP$_{aq}$ as oxidant, the use of MeCN as solvent instead of TFT had a detrimental effect (15% and 0% conversion, respectively, at 6 h/70°C) (Table 1). ATR FT-IR spectroscopy indicated that ODC was incomplete within 24 h at 70°C for the system TBHP/MeCN (in parallel to that found for TBHP/TFT) (Figure 12). The incomplete ODC for MeCN, together with the fact that this solvent has coordinating properties, may contribute to the poor catalytic performance.

Changing the type of oxidant from TBHP to hydrogen peroxide impacted negatively on the catalytic reaction kinetics. Specifically, the systems H_2O_2/MeCN and H_2O_2/H_2O led to 39% and 0% Cy8 conversion, respectively, at 24 h/70°C (Table 1). Comparing H_2O_2/H_2O with TBHP$_{aq}$/H_2O (0% and 61% conversion, respectively, at 24 h) suggests that the negative impact of water does not solely explain the catalytic results with H_2O_2 as oxidant. Possibly, the distributions of metal species may be different for the different oxidants.

As mentioned above, **1**@CB7 and **1**@CB8 are the first inclusion compounds based on CB hosts and organomolybdenum guests studied as supramolecular catalysts for the Cy8/TBHP model reaction. Table 2 compares the catalytic results for these compounds to literature data for inclusion compounds based on CD hosts with molybdenum complexes tested for the Cy8/TBHP reaction.[14–16,38] Some of the reported studies used a greater amount of catalyst or oxidant (relative to the olefin) than that used for **1**@CB7 and **1**@CB8. For example, $CpMo(CO)_3CH_2CONH_2$@β-CD was tested using an initial Mo:olefin:oxidant molar ratio of 1:50:78 (1,2-dichloroethane as solvent, entry 6),[14] and MoO_2Cl_2(FcNN)@TRIMEB (FcNN = *N,N′*-bis(ferrocenylmethylene)ethylenediamine) was tested using a 1:100:200 ratio (without cosolvent, entry 9)[38]; the two compounds led to 100% epoxide yield after 24 h reaction at 55°C or 70°C. Based on conversion (discarding the differences in reaction conditions), the results for **1**@CB7 are comparable with those reported for the (stable) inclusion

TABLE 1 Influence of reaction conditions on the performance of **1**@CB8 for Cy8 epoxidation.[a]

Oxidant	Solvent	*T* (°C)	*t* (h)	Conv. (%)[b]	Select. (%)[c]
TBHP	TFT	70	24 (run 1/run 2/run 3)	62/58/65	100/100/100
TBHP	TFT	90	24 (run 1/run 2/run 3)	85/81/87	83/84/78
$TBHP_{aq}$	TFT	70	24 (run 1/run 2/run 3)	57/40/35	100/100/100
$TBHP_{aq}$	TFT	90	24 (run 1/run 2/run 3)	71/59/53	100/90/79
$TBHP_{aq}$	H_2O	70	24 (run 1/run 2/run 3)	61/39/32	100/100/88
TBHP	MeCN	70	6	15	100
$TBHP_{aq}$	MeCN	70	6	0	0
H_2O_2	MeCN	70	24	39	100
H_2O_2	H_2O	70	24	0	0

Abbreviations: TBHP, *tert*-butylhydroperoxide in decane; $TBHP_{aq}$, aqueous *tert*-butylhydroperoxide; TFT, α,α,α-trifluorotoluene; *T*, reaction temperature; *t*, reaction time.
[a]Initial Mo:olefin:oxidant molar ratio = 1:100:153.
[b]Conv. = Cy8 conversion.
[c]Select. = selectivity to cyclooctene oxide at the indicated conversions.

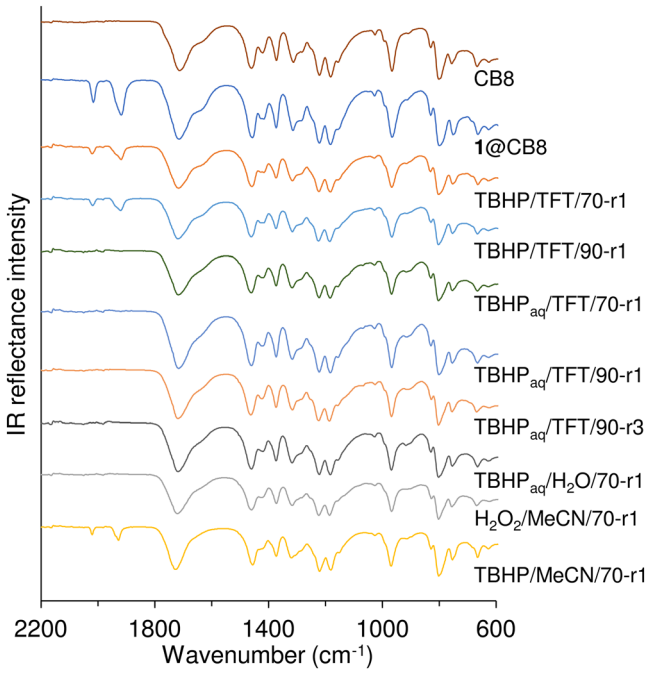

FIGURE 12 Attenuated total reflectance FT-IR spectra in the range of 600–2200 cm^{-1} of CB8, the inclusion compound **1**@CB8, and solids recovered after Cy8O epoxidation reactions performed for 24 h. The term *T*-r*i* indicates the reaction temperature (*T*) and the run number (*i*). TBHP, *tert*-butylhydroperoxide in decane; $TBHP_{aq}$, aqueous *tert*-butylhydroperoxide; TFT, α,α,α-trifluorotoluene.

compound with β-CD as host and the organometallic complex $CpMo(CO)_3CH_2CONH_2$ as guest (entry 5) which led to 82% epoxide yield.[14] Nevertheless, the reaction conditions were very different, and the two compounds have hosts with different cavity sizes (CB7 with 5.4 Å; β-CD with 6.0–6.5 Å) and guests with different Mo coordination spheres, which may influence the reaction kinetics. On the other hand, some of the reported inclusion compounds suffered partial loss of activity (when reused),[15] while other studies were not focused on catalytic stability,[38] making fair comparisons difficult.

The catalytic performances of **1**@CB7 and **1**@CB8 were further investigated for the epoxidation of bulky substrate molecules, namely, cyclododecene (Cy12) and the biomass-derived olefin MeOle, at 90°C using the TBHP/TFT system. The two inclusion compounds led to similar Cy12 conversion at 24 h (58–61%). The kinetic diameter of Cy12 is ~8 Å,[39] which is greater than the portal sizes of CB7 and CB8 (~5.4 and 6.9 Å, respectively). With MeOle as substrate, which is a relatively large fatty acid methyl ester (~25 Å along the C–C segments, 5 Å for the cross section),[40] **1**@CB7 was inactive, while **1**@CB8 led to 33% conversion at 24 h. The fact that **1**@CB7 led to higher activity than **1**@CB8 with Cy8 as substrate, similar activity with Cy12, and inferior activity with MeOle suggests that steric effects become important for reactions of relatively bulky olefins. Substrate exclusion due to cavity size restrictions was previously reported for an oxovanadium(VI)-CB6 heterogeneous oxidation catalyst.[41] With H_2O_2 as oxidant, the catalyst was not able to oxidize Cy8, which has larger molecular dimensions than the CB6 portal size.

Based on the ATR FT-IR spectra of the recovered solids, the ODC seemed faster for **1**@CB7 than for **1**@CB8 for the three substrates (Figure 8). Concerning the selectivity of the Cy12 and MeOle reactions, different distributions of products were obtained, in agreement with that observed for the Cy8 reaction. The reaction of Cy12 in the presence of **1**@CB7 led to cyclododecene oxide as the only product, whereas **1**@CB8 led to 1,2-cyclododecanediol as a byproduct (15% selectivity) in

TABLE 2 Comparison of the catalytic results for **1**@CB7 and **1**@CB8 to literature data for inclusion compounds based on cyclodextrin (CD) hosts with molybdenum complexes, tested for the Cy8/*tert*-butylhydroperoxide reaction.

Entry	Catalyst	H:G[a]	Mo:Ol:Ox[b]	Solv.	*T* (°C)	Conv. (%)[c]	Ref.
1	**1**@CB7	1:1	1:100:153	TFT	70	85	This work
2	**1**@CB8	1:1	1:100:153	TFT	70	62	This work
3	$CpMo(CO)_3Cl$@β-CD	1:1	1:100:100	ns	55	98	15
4	$CpMo(CO)_3Cl$@TRIMEB	1:1	1:100:100	ns	55	95	15
5	$CpMo(CO)_3CH_2CONH_2$@β-CD	5:1	1:50:78	ns	55	82	14
6	$CpMo(CO)_3CH_2CONH_2$@β-CD	5:1	1:50:78	DCE	55	100	14
7	$CpMo(CO)_3CH_2CONH_2$@TRIMEB	1:1	1:50:78	ns	55	100	14
8	$CpMo(CO)_3CH_2CONH_2$@TRIMEB	1:1	1:50:78	DCE	55	100	14
9	MoO_2Cl_2(FcNN)@TRIMEB	2:1	1:100:200	ns	70	100	38
10	$CpMo(CO)_3(CH_2\text{-}pC_6H_4\text{-}CO_2CH_3)$@DIMEB	1:1	1:100:150	ns	55	96	16
11	$CpMo(CO)_3(CH_2\text{-}pC_6H_4\text{-}CO_2CH_3)$@TRIMEB	1:1	1:100:150	ns	55	100[d]	16

Abbreviations: β-CD, β-cyclodextrin; DCE, 1,2-dichloroethane; DIMEB, heptakis(2,6-di-*O*-methyl)-β-CD; FcNN, diimine ligand *N*,*N*′-bis(ferrocenylmethylene) ethylenediamine; ns, no solvent; Solv., solvent; *T*, reaction temperature; TFT, α,α,α-trifluorotoluene; TRIMEB, heptakis(2,3,6-tri-*O*-methyl)-β-CD.

[a]The host:guest molar ratio in the inclusion complex.

[b]Mo:olefin:oxidant molar ratio.

[c]Conv. = Cy8 conversion at 24 h unless otherwise indicated. Selectivity to the epoxide was 100% in all cases.

[d]Reaction time = 3 h.

addition to the epoxide (85% selectivity). On the other hand, the reaction of MeOle in the presence of **1**@CB8 led to approximately equimolar amounts of methyl 9,10-epoxyoctadecanoate and methyl 10-oxooctadecanoate (47% and 53% selectivity, respectively) at 24 h.

4 | CONCLUSIONS

In this work, for the first time, inclusion compounds based on CB hosts and organomolybdenum guests were studied as supramolecular catalysts for olefin epoxidation. The compounds **1**@CB*n*, synthesized via encapsulation of the carbonyl complex $[CpMo(CO)_3Me]$ (**1**) in CB*n* ($n = 7$ and 8), promoted the heterogeneous catalytic epoxidation of olefins with TBHP. The catalytic performance was strongly influenced by the reaction conditions (temperature, oxidant, and solvent) and the structural features of the compounds. In general, increasing the reaction temperature led to faster kinetics, whereas coordinating solvents (MeCN and water) led to poorer catalytic performance. **1**@CB8 was less selective toward the epoxide products than **1**@CB7 at 90°C, but the former was more stable in consecutive batch runs (at 70°C or 90°C). The structural features (e.g., portal sizes) of the supramolecular compounds may be determinant, especially for the epoxidation of relatively bulky olefins such as cyclododecene and the biomass-derived MeOle (e.g., **1**@CB8 led to MeOle conversion, whereas **1**@CB7 was inactive). These results suggest that Mo@CB*n*-type host–guest complexes merit future work on the encapsulation of different types of metal species in the CB*n* containers and the application of the resultant compounds in selective catalytic oxidation systems.

AUTHOR CONTRIBUTIONS

Patrícia Neves: Investigation; validation; visualization; writing—original draft. **Ana C. Gomes:** Investigation; validation; visualization; writing—original draft. **Rodrigo P. Monteiro:** Investigation; validation; visualization; writing—original draft. **Mirela J. Santos:** Validation; writing—review and editing. **Anabela A. Valente:** Conceptualization; project administration; resources; supervision; writing—review and editing. **André D. Lopes:** Investigation; validation. **Isabel S. Gonçalves:** Conceptualization; project administration; resources; supervision. **Martyn Pillinger:** Resources; validation; visualization; writing—review and editing.

ACKNOWLEDGMENTS

This work was carried out with the support of CICECO - Aveiro Institute of Materials (UIDB/50011/2020, UIDP/50011/2020, and LA/P/0006/2020), financed by national funds through the FCT/MCTES (PIDDAC). The NMR spectrometers used in this work are part of the National NMR Network (PTNMR) and are partially supported by Infrastructure Project No. 022161 (cofinanced by FEDER through COMPETE 2020, POCI and PORL, and FCT through PIDDAC). A. C. G. is grateful to the FCT/MCTES for an Assistant Researcher Position

(CEECIND/02128/2017) funded through the Individual Call to Scientific Employment Stimulus. R. P. M. thanks the FCT and the European Social Fund for a PhD grant (ref. 2020.04758.BD).

CONFLICT OF INTEREST STATEMENT

All authors declare that there are no conflicts of interest.

DATA AVAILABILITY STATEMENT

The data that support the findings of this study are available in the main text and from the corresponding authors upon reasonable request.

REFERENCES

[1] B. Cornils, W. A. Herrmann, *J. Catal.* **2003**, *216*, 23. https://doi.org/10.1016/S0021-9517(02)00128-8

[2] I. Melián-Cabrera, *Ind. Eng. Chem. Res.* **2021**, *60*, 18545. https://doi.org/10.1021/acs.iecr.1c02681

[3] C. J. Elsevier, J. Reedijk, P. H. Walton, M. D. Ward, *Dalton Trans.* **2003**, 1869. https://doi.org/10.1039/B303975G

[4] W. Matsuoka, Y. Harabuchi, S. Maeda, *ACS Catal.* **2023**, *13*, 5697. https://doi.org/10.1021/acscatal.3c00576

[5] J. N. H. Reek, B. de Bruin, S. Pullen, T. J. Mooibroek, A. M. Kluwer, X. Caumes, *Chem. Rev.* **2022**, *122*, 12308. https://doi.org/10.1021/acs.chemrev.1c00862

[6] M. Raynal, P. Ballester, A. Vidal-Ferran, P. W. N. M. van Leeuwen, *Chem. Soc. Rev.* **2014**, *43*, 1734. https://doi.org/10.1039/c3cs60037h

[7] S. H. A. M. Leenders, R. Gramage-Doria, B. de Bruin, J. N. H. Reek, *Chem. Soc. Rev.* **2015**, *44*, 433. https://doi.org/10.1039/c4cs00192c

[8] J. R. Moran, S. Karbach, D. J. Cram, *J. Am. Chem. Soc.* **1982**, *104*, 5826. https://doi.org/10.1021/ja00385a064

[9] P. D. Frischmann, M. J. MacLachlan, *Chem. Soc. Rev.* **2013**, *42*, 871. https://doi.org/10.1039/C2CS35337G

[10] N. A. F. Al-Rawashdeh, A. M. Al-Ajlouni, S. B. Bukallah, N. Bataineh, *J. Inclusion Phenom. Macrocyclic Chem.* **2011**, *70*, 471. https://doi.org/10.1007/s10847-010-9876-3

[11] T. G. Brevé, M. Filius, C. Araman, M. P. van der Helm, P.-L. Hagedoorn, C. Joo, S. I. van Kasteren, R. Eelkema, *Angew. Chem., Int. Ed.* **2020**, *59*, 9340. https://doi.org/10.1002/anie.202001369

[12] E. T. Luis, A. I. Day, B. König, J. E. Beves, *Inorg. Chem.* **2020**, *59*, 9135. https://doi.org/10.1021/acs.inorgchem.0c00986?ref=pdf

[13] M. A. Sarmentero, H. Fernández-Pérez, E. Zuidema, C. Bo, A. Vidal-Ferran, P. Ballester, *Angew. Chem., Int. Ed.* **2010**, *49*, 7489. https://doi.org/10.1002/anie.201003026

[14] S. S. Braga, S. Gago, J. D. Seixas, A. A. Valente, M. Pillinger, T. M. Santos, I. S. Gonçalves, C. C. Romão, *Inorg. Chim. Acta* **2006**, *359*, 4757. https://doi.org/10.1016/j.ica.2006.03.017

[15] S. S. Balula, A. C. Coelho, S. S. Braga, A. Hazell, A. A. Valente, M. Pillinger, J. D. Seixas, C. C. Romão, I. S. Gonçalves, *Organometallics* **2007**, *26*, 6857. https://doi.org/10.1021/om701025z

[16] A. C. Gomes, S. M. Bruno, C. Tomé, A. A. Valente, M. Pillinger, M. Abrantes, I. S. Gonçalves, *J. Organomet. Chem.* **2013**, *730*, 116. https://doi.org/10.1016/j.jorganchem.2012.12.019

[17] M. K. Trost, R. G. Bergman, *Organometallics* **1991**, *10*, 1172. https://doi.org/10.1021/om00050a058

[18] A. M. Al-Ajlouni, D. Veljanovski, A. Capapé, J. Zhao, E. Herdtweck, M. J. Calhorda, F. E. Kühn, *Organometallics* **2009**, *28*, 639. https://doi.org/10.1021/om8009206

[19] S. M. Bruno, A. C. Gomes, T. S. M. Oliveira, M. M. Antunes, A. D. Lopes, A. A. Valente, I. S. Gonçalves, M. Pillinger, *Org. Biomol. Chem.* **2016**, *14*, 3873. https://doi.org/10.1039/c6ob00512h

[20] A. C. Gomes, C. I. R. Magalhães, T. S. M. Oliveira, A. D. Lopes, I. S. Gonçalves, M. Pillinger, *Dalton Trans.* **2016**, *45*, 17042. https://doi.org/10.1039/c6dt02811j

[21] M. Abrantes, P. Neves, M. M. Antunes, S. Gago, F. A. Almeida Paz, A. E. Rodrigues, M. Pillinger, I. S. Gonçalves, C. M. Silva, A. A. Valente, *J. Mol. Catal. A: Chem.* **2010**, *320*, 19. https://doi.org/10.1016/j.molcata.2009.12.011

[22] T. S. Piper, G. Wilkinson, *J. Inorg. Nucl. Chem.* **1956**, *3*, 104. https://doi.org/10.1016/0022-1902(56)80073-0

[23] D. P. Buck, P. M. Abeysinghe, C. Cullinane, A. I. Day, J. G. Collins, M. H. Harding, *Dalton Trans.* **2008**, 2328. https://doi.org/10.1039/B718322D

[24] M. J. Calhorda, *Chem. Commun.* **2000**, 801. https://doi.org/10.1039/A900221I

[25] S. S. Braga, I. S. Gonçalves, A. D. Lopes, M. Pillinger, J. Rocha, C. C. Romão, J. J. C. Teixeira-Dias, *Dalton Trans.* **2000**, 2964. https://doi.org/10.1039/b003763j

[26] S. Lima, I. S. Gonçalves, P. Ribeiro-Claro, M. Pillinger, A. D. Lopes, P. Ferreira, J. J. C. Teixeira-Dias, J. Rocha, C. C. Romão, *Organometallics* **2001**, *20*, 2191. https://doi.org/10.1021/om001088s

[27] S. A. Hauser, R. M. Reich, J. Mink, A. Pöthig, M. Cokoja, F. E. Kühn, *Catal. Sci. Technol.* **2015**, *5*, 2282. https://doi.org/10.1039/C4CY01604A

[28] C. J. Stephenson, J. T. Hupp, O. K. Farha, *Inorg. Chem. Front.* **2015**, *2*, 448. https://doi.org/10.1039/C5QI00010F

[29] S. Funk, J. Schatz, *J. Inclusion Phenom. Macrocyclic Chem.* **2020**, *96*, 1. https://doi.org/10.1007/s10847-019-00956-0

[30] T. Ma, C. Xu, F. Liu, Y. Feng, W. Zhang, W. Tang, H. Zhang, X. Li, Y. Nie, S. Zhao, Y. Li, D. Ji, Z. Fang, W. He, K. Guo, *Mol. Catal.* **2023**, *541*, 113074. https://doi.org/10.1016/j.mcat.2023.113074

[31] P. J. Costa, M. J. Calhorda, F. E. Kühn, *Organometallics* **2010**, *29*, 303. https://doi.org/10.1021/om9002522

[32] M. J. Calhorda, P. J. Costa, *Curr. Org. Chem.* **2012**, *16*, 65. https://doi.org/10.2174/138527212798993095

[33] J. Zhao, A. M. Santos, E. Herdtweck, F. E. Kühn, *J. Mol. Catal. A: Chem.* **2004**, *222*, 265. https://doi.org/10.1016/j.molcata.2004.07.023

[34] N. Grover, A. Pöthig, F. E. Kühn, *Catal. Sci. Technol.* **2014**, *4*, 4219. https://doi.org/10.1039/C4CY00738G

[35] N. Grover, M. Drees, F. E. Kühn, *J. Catal.* **2015**, *329*, 269. https://doi.org/10.1016/j.jcat.2015.05.019

[36] P. Neves, *Catalisadores ou precursores de espécies activas à base de molibdénio*, PhD Thesis, University of Aveiro **2011**.

[37] C. Dino, M. Ciclosi, E. Manoury, L. Maron, L. Perrin, R. Poli, *Chem. – Eur. J.* **2010**, *16*, 9572. https://doi.org/10.1002/chem.201000298

[38] Ž. Petrovski, S. S. Braga, A. M. Santos, S. S. Rodrigues, I. S. Gonçalves, M. Pillinger, F. E. Kühn, C. C. Romão, *Inorg. Chim. Acta* **2005**, *358*, 981. https://doi.org/10.1016/j.ica.2004.11.032
[39] D. Yu, W. Gao, S. Xing, L. Lian, H. Zhang, X. Wang, D. Lou, *RSC Adv.* **2019**, *9*, 4884. https://doi.org/10.1039/C8RA10388G
[40] M. Dvoyashkin, N. Wilde, J. Haase, R. Gläser, *RSC Adv.* **2018**, *8*, 38941. https://doi.org/10.1039/C8RA07434H
[41] S. M. de Lima, J. A. Gómez, V. P. Barros, G. D. S. Vertuan, M. D. D. Assis, C. F. D. O. Graeff, G. J.-F. Demets, *Polyhedron* **2010**, *29*, 3008. https://doi.org/10.1016/j.poly.2010.08.001

How to cite this article: P. Neves, A. C. Gomes, R. P. Monteiro, M. J. Santos, A. A. Valente, A. D. Lopes, I. S. Gonçalves, M. Pillinger, *Appl Organomet Chem* **2024**, e7412. https://doi.org/10.1002/aoc.7412